Proceedings of the
Annual Stability Conference
Structural Stability Research Council
Denver, Colorado, March 22-25 2022

Nonlinear dynamic analysis and fragility development of electrical transmission towers under hurricanes

Xinlong Du[1], Jerome F. Hajjar[2]

Abstract

Electrical transmission towers are usually made of slender single angle members, which are prone to have flexural and flexural-torsional buckling behaviors under large deformations. In this research, both displacement-based and mixed beam elements are developed and implemented in the OpenSees software for simulating elastic and inelastic buckling of members with asymmetric sections such as steel angles and tees. Geometric nonlinearity is captured using a corotational total Lagrangian approach, while material nonlinearity is modeled using the fiber section method with uniaxial constitutive laws. The formulations try to minimize the number of elements needed through remedying membrane locking, representing nonlinear curvature within an element, and utilizing a kinematic model in the basic system that decouples axial, flexural, and torsional deformations for the first order effect. This research then proposes a procedure for developing collapse fragility curves of transmission towers subjected to hurricanes. The storm maximum gust speed is selected as the intensity measure and incremental dynamic analysis (IDA) is adopted to model collapse with the use of the newly developed beam element. Uncertainties in wind speeds, directions and durations are considered by running IDAs on transmission towers with a suite of hurricane wind records. The fragility curve is assumed to be the cumulative distribution function of the intensity measure at the onset of collapse. The parameters of the fragility curve are estimated by employing the method of moments with a premise that the intensity measure at the onset of collapse follows a lognormal distribution.

1. Introduction

Electrical transmission towers are vulnerable to hurricane winds. For example, Hurricane Katrina broke 402 cable support towers in Mississippi, which lead to about 200,000 customers lost their power (Cauffman et al., 2006). Therefore, performance and reliability of transmission towers should be thoroughly studied so that the damage of these structures can be quickly estimated, which can benefit emergency management of transmission networks during hurricanes. This research focus on development of collapse fragility of transmission towers subjected highly intensive winds due to hurricanes. This goal is achieved through developing finite element method for modeling nonlinear behavior of transmission towers, selecting appropriate hurricane wind

[1] Graduate Research Assistant, Northeastern University, <du.xinl@northeastern.edu>
[2] CDM Smith Professor and Chair, Northeastern University, <jf.hajjar@northeastern.edu>

records with considering uncertainties in different hurricanes, conducting incremental dynamic analysis (IDA) for estimating the collapse capacity of transmission towers, and generating collapse fragility curves using a set of simulated data of the collapse capacity.

Conventional transmission towers are made of slender steel angles, which are monosymmetric or asymmetric. Members manufactured from these sections usually have coupled axial-flexural-torsional deformation due to the noncoincident centroid and shear center, and the Wagner effect. Therefore, it is critical to accurately simulate this axial-flexural-torsional coupling phenomenon of steel angles so that the real behavior of transmission towers under large deformation can be captured. In addition, collapse fragility curves of transmission towers are of interest, which means that parts of the structure should be in plastic stage and the material nonlinear behavior of the angle members should be modeled. To account for the above mentioned geometric nonlinear effects, displacement-based and mixed beam elements are developed within the corotational total Lagrangian formulation, while the material nonlinear effect is considered using a fiber section analysis approach. The total Lagrangian method is invoked within a basic coordinate system that continuously translates and rotates with the element. The rigid body motion is considered through the corotational transformation and the high order terms in the strain displacement compatibility equation are included in the basic system to model the axial-flexural-torsional interaction. Compared with the conventional total and updated Lagrangian formulations without corotational transformation, the corotational formulation can reduce the number of degrees-of-freedom (DOFs); therefore, the element formulation is simplified. The kinematic model used in the basic system follows the classical beam theory where bending is defined with respect to the centroid and torsion is referred to the shear center. A linear transformation is then adopted to move all degrees-of-freedom to the shear center in advance to the corotational transformation. The beam elements are implemented in the OpenSees framework (McKenna et al., 2010), validated with a set of examples, and then used for nonlinear dynamic analysis of transmission towers.

The collapse fragility development includes running a series of IDAs (Vamvatsikos and Cornell, 2002) with a set of hurricane wind records selected from a synthetic hurricane catalog (Liu, 2014) to consider the record-to-record randomness. From the perspective of structural reliability, fragility is defined as the failure probability of a structure conditional on a given loading intensity. Here, the hazard intensity measure is set to be the storm-maximum gust wind speed. The limit state that is considered in the fragility development is collapse, which is related to global dynamic stability of the tower and is determined by using IDA. The fragility curve is modeled as the cumulative distribution function (CDF) of a lognormal distribution, and the two parameters of the CDF are estimated using the method of moments.

2. Beam Element Development for Angle Sections

This section presents the development and validation of the displacement-based and mixed beam elements in OpenSees, which can be used to simulate the nonlinear behavior of angle members used in transmission towers. Both the displacement-based element and the mixed element can address inelastic behavior using fiber-based cross section formulations. The mixed element has more complex formulations and is more computationally intensive than the displacement-based element; however, the mixed element can model nonlinear curvature within an element while the displacement-based element is only capable of representing linear curvature. Consequently, for severely inelastic cases with nonlinear distribution of curvature such as plastic hinges, the mixed

element is more accurate, and fewer number of mixed elements are needed to obtain similar results as compared to the displacement-based element.

2.1 Corotational Total Lagrangian Framework

To capture the axial-flexural-torsional interaction behaviors of slender members with asymmetric sections such as steel angles, the Green-Lagrange strain is invoked by using the total Lagrangian approach in the basic system of the corotational transformation approach. Within the context of corotational transformation, when describing strains and displacements at time $t+\Delta t$, the reference system is selected as the basic system at time $t+\Delta t$ (i.e., reference configuration in Fig. 1). The element with 6 DOFs is formulated in the basic system at time $t+\Delta t$, which is then transformed to the 12-DOF global system with the help of the corotational transformation matrix at time $t+\Delta t$. The corotational transformation matrix is time dependent since the basic system translates and rotates continuously with the moving element chord. The pure deformations are captured at the basic system, while the rigid body motions are considered using the transformation matrix relating the global and basic coordinate systems.

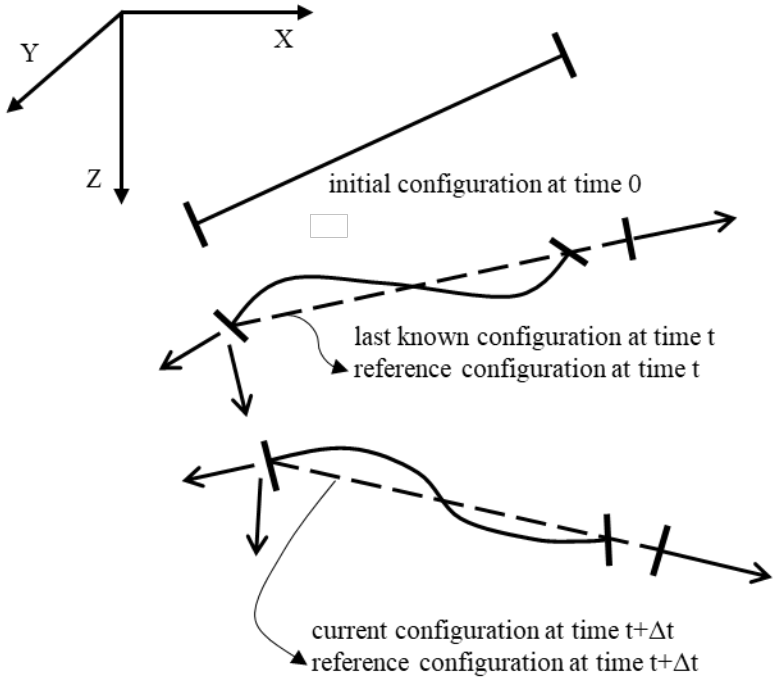

Figure 1. Global and basic systems of the corotational total Lagrangian formulation (after Mattiasson et al., 1985)

2.2 Coordinate Systems

Since the new elements are implemented in the OpenSees framework, the same global system and corotational transformation from the original OpenSees element are adopted. However, due to the noncoincident shear center and centroid of the beam element with asymmetric sections such as steel angles, the basic coordinate system is slightly different from the one used in typical beam elements in OpenSees. Figure 2 shows an angle section in the basic system, which is defined with two coordinate systems: x, y, z and $\boldsymbol{x}$, $\boldsymbol{y}$, $\boldsymbol{z}$. The right-hand orthogonal coordinate system x, y, z is selected such that y and z are the principal axes of the cross section and x is the centroidal axis CC'. the coordinate system $\boldsymbol{x}$, $\boldsymbol{y}$, $\boldsymbol{z}$ is defined such that $\boldsymbol{y}$ and $\boldsymbol{z}$ are parallel to the principal axes (y and z) of the cross section and $\boldsymbol{x}$ is the shear center axis SS'. In this formulation, v and w represent

displacements of the shear center in the $\boldsymbol{y}$ and $\boldsymbol{z}$ directions, respectively, u is the axial displacement along the centroidal axis, and ϕ is the angle of twist about the shear center axis. This new basic system uncouples axial, flexural, and torsional deformations for the first-order effect.

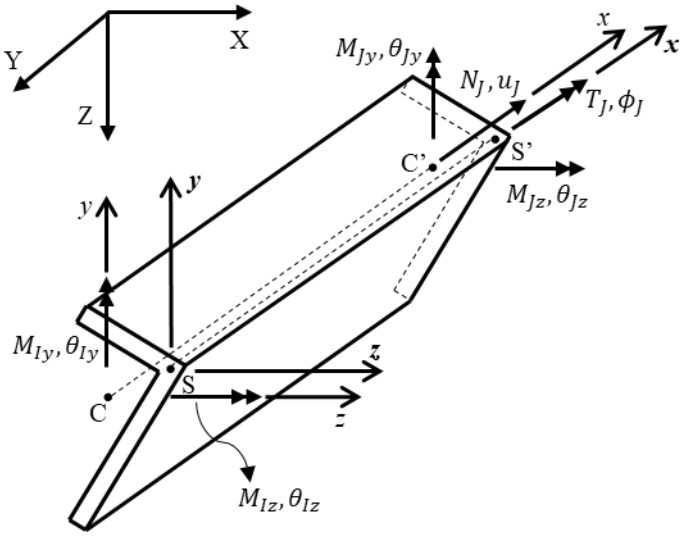

Figure 2: Element nodal forces and reference axes in the basic system

In the basic system, the element stiffness matrix is formulated, which has 6 DOFs: one relative axial displacement u_J of the centroids, two rotations relative to the chord θ_{Iz} and θ_{Jz}, about the z axis, two rotations relative to the chord θ_{Iy} and θ_{Jy}, about the y axis, and one relative angle of twist ϕ_J about the $\boldsymbol{x}$ axis. The corresponding nodal forces are the axial force N_J acting along the centroidal axis; the two bending moments acting about the principal axis z and in the $\boldsymbol{xy}$ plane, M_{Iz} and M_{Jz}; the two bending moments acting about the principal axis y and in the $\boldsymbol{xz}$ plane, M_{Iy} and M_{Jy}; and the torque T_J acting about the shear center axis. These nodal displacements and forces are expressed in vector format as

$$\boldsymbol{D}_b = [u_J \quad \theta_{Iz} \quad \theta_{Jz} \quad \theta_{Iy} \quad \theta_{Jy} \quad \phi_J]^T \tag{1}$$

and

$$\boldsymbol{P}_b = [N_J \quad M_{Iz} \quad M_{Jz} \quad M_{Iy} \quad M_{Jy} \quad T_J]^T \tag{2}$$

When using the corotational transformation approach, nodal displacements, nodal forces, and the stiffness matrix should be transformed to the global system. Nevertheless, within the current basic system, some DOFs are defined about the shear center, while others are defined with respect to the centroid. This means that the conventional corotational transformation should not be applied directly. Therefore, all nodal forces and displacements must be transformed to the same reference point before the corotational transformation. In the basic system, the lateral forces and torque are referred to the shear center, the moments act in the planes containing the shear center, while the axial force is defined with respect to the centroid. Consequently, it is straightforward to transform all DOFs to act about the shear center, since only the axial force needs to be transformed. If another point (e.g., the centroid) is chosen as the reference point, then the lateral forces also need to be transformed, which is more difficult, since the lateral forces are only recovered after the corotational transformation. Thus, it is appropriate to select the shear center as the reference point and select the shear center axis as the member reference axis in advance of the corotational

transformation. The coordinate system $\boldsymbol{x}$, $\boldsymbol{y}$, $\boldsymbol{z}$ is referred as the element basic reference system with the nodal displacements $\boldsymbol{D}_r$ and forces $\boldsymbol{P}_r$ acting about the shear center. The equations adopted to transform all DOFs to shear center are shown as

$$\boldsymbol{P}_r = \boldsymbol{T}_r^T \boldsymbol{P}_b \tag{3}$$

and

$$\boldsymbol{D}_b = \boldsymbol{T}_r \boldsymbol{D}_r \tag{4}$$

where the cross-sectional transformation matrix is defined as (Richen et al., 2020)

$$\boldsymbol{T}_r^T = \begin{bmatrix} 1 & 0 & 0 & 0 & 0 & 0 \\ y_s & 1 & 0 & 0 & 0 & 0 \\ -y_s & 0 & 1 & 0 & 0 & 0 \\ -z_s & 0 & 0 & 1 & 0 & 0 \\ z_s & 0 & 0 & 0 & 1 & 0 \\ 0 & 0 & 0 & 0 & 0 & 1 \end{bmatrix} \tag{5}$$

and y_s and z_s are coordinates of the shear center with respect to the centroid. Therefore, in the element basic reference system, the tangent stiffness matrix is

$$\boldsymbol{K}_r = \boldsymbol{T}_r^T \boldsymbol{K}_b \boldsymbol{T}_r \tag{6}$$

where $\boldsymbol{K}_b$ is the element tangent stiffness matrix in the basic system.

2.3 Beam Section Kinematics

With the kinematic assumption of the Euler-Bernoulli beam theory and neglecting warping effects, the motion of a material point P (x, y, z), which is defined in the coordinate system x, y, z in Fig. 2, on the cross section is described in terms of the displacement components of the shear center and centroid (Alemdar, 2001; Trahair, 1993)

$$u_p = u - yv' - zw' + z\phi v' - y\phi w' \tag{7}$$

$$v_p = v - \phi(z - z_s) \tag{8}$$

$$w_p = w + \phi(y - y_s) \tag{9}$$

where y_s, z_s, u, v, w and ϕ are defined in Section 2.2. Taking derivatives of the displacement fields in Eq. (7) to Eq. (9) with respect to x and substituting the results into the definition of the Green-Lagrange strain gives

$$\hat{\varepsilon} = u' - yv'' - zw'' + \frac{1}{2}[(v')^2 + (w')^2] + \frac{1}{2}[(y - y_s)^2 + (z - z_s)^2](\phi')^2 + (z_s v' - y_s w')\phi' + (zv'' - yw'')\phi \tag{10}$$

Comparing with the axil strain term $\hat{\varepsilon} = u' - yv'' - zw''$ adopted in the original OpenSees beam element, Eq. (10) has extra terms that can account for the coupling between the axial, flexural and torsional deformations. The shear strain at the material point P resulting from twisting of a member with thin-walled open section is approximated by the following equation (Rasmussen, 1997)

$$\hat{\gamma} = 2n\phi' \tag{11}$$

where n is the perpendicular distance between the material point P and the mid-thickness line of the cross-section. Shear strains due to bending and warping torsion are ignored.

2.4 Element Formulation

The displacement-based beam element can be derived from the principle of virtual work, which is

$$\int_{V_0} \delta\hat{\boldsymbol{\epsilon}}^T \boldsymbol{\sigma}\, dV - \delta \boldsymbol{D}_b^T \boldsymbol{P}_{ext} = 0 \tag{12}$$

where $\hat{\boldsymbol{\epsilon}} = [\hat{\varepsilon} \quad \hat{\gamma}]^T$ is the strain vector, $\boldsymbol{\sigma} = [\sigma \quad \tau]^T$ is the corresponding stress vector, V_0 is the volume of the undeformed element, and $\boldsymbol{P}_{ext}$ is a vector of external forces acting on element ends.

The mixed element can be derived from the Hellinger-Reissner variational principle, which can be stated by combining Eq. (12) of equilibrium and Eq. (13) of compatibility (Alemdar, 2001).

$$\int_{l_0} \delta \boldsymbol{S}^T \left(\widehat{\boldsymbol{d}} - \boldsymbol{d}\right) dx = 0 \tag{13}$$

In Eq. (13), l_0 is the length of the undeformed element, $\boldsymbol{S}$ is the stress resultant internal force vector, $\widehat{\boldsymbol{d}}$ is the cross-section deformation vector derived from displacement fields, and $\boldsymbol{d}$ is the cross-section deformation vector derived from the interpolated stress resultant internal force fields ($\boldsymbol{S}$). The derivation of the displacement-based element requires appropriate displacement shape functions, while the derivation of the mixed element requires both displacement and force shape functions. Here, cubic shape functions are adopted for the transverse deflections so one displacement-based element can only represent a linear curvature field, while the mixed element can model nonlinear curvature within an element because of using both displacement and force shape functions in the Hellinger-Reissner variational principle. After linearization of the weak form of the governing equations (Eq. (12) for the displacement-based element; Combination of Eq. (12) and Eq. (13) for the mixed element), the following iteration format can be obtained

$$\boldsymbol{K}_b \Delta \boldsymbol{D}_b = \boldsymbol{P}_{ext}^{i+1} - \boldsymbol{P}_{int}^{i} \tag{14}$$

where $\Delta \boldsymbol{D}_b$ is the increment of element end displacement; $\boldsymbol{P}_{ext}^{i+1}$ and $\boldsymbol{P}_{int}^{i}$ are the external load vector in $(i+1)^{\text{th}}$ iteration and the element internal resisting forces in i^{th} iteration, respectively. In addition, to remedy the membrane locking problem of the displacement-based element, the high order strain term $\frac{1}{2}[(v')^2 + (w')^2]$ appeared in Eq. (10) is replaced by an effective membrane strain $\frac{1}{l_0}\int_0^{l_0} \frac{1}{2}[(v')^2 + (w')^2]\, dx$ as suggested by Crisfield (1991, 1997), while the mixed element does not have this problem as demonstrated in the examples in Section 2.5.

2.5 Validation Examples

In the following examples, "DBxx" indicates using xx number of the new displacement-based element with membrane locking remedied, while "MBxx" indicates using xx number of the new mixed elements.

2.5.1 Eccentrically Loaded Beam-Column

This example, previously studied by Alemdar (2001), is about a simply supported beam-column subjected to an eccentric axial load (see Fig. 3). The length of the beam-column is L = 6668.52 mm, and the eccentricity is e = 20.83 mm. The beam-column is in strong axis bending. The bending stiffness is EI and the axial load is $P = 8EI/L^2$. As for the material properties, Young's modulus E is 199,948 MPa and Poisson's ratio v is 0.3.

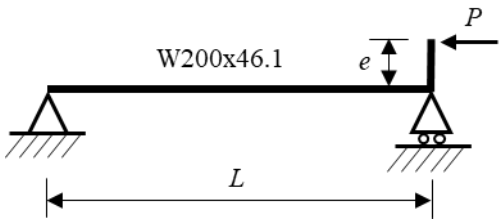

Figure 3. Eccentrically loaded beam-column

To simulate this example, 1 displacement-based element with membrane locking remedied and 1 mixed element are adopted with elastic material. In Fig. 4, the exact curvature field along the member is compared with the curvature values at the Gauss integration points obtained from the

displacement-based and mixed elements. It is seen that the displacement-based element can only represent a linear curvature field owing to the cubic shape functions used for transverse deflections. In contrast, the mixed element exhibits a nonlinear curvature field because of the independently interpolated displacement fields and force fields. Equilibrium is satisfied at each Gauss integration point within the mixed element, while it is only satisfied in a weighted average sense for the displacement-based element. This example is also simulated using 2 elements whose results are illustrated in Fig. 5. The mixed element yields a good approximation for the nonlinear curvature field with no discontinuity, while the curvature field of the displacement-based element includes two linear parts with a discontinuity at the connection point. In this example, each element has seven Gauss-Lobatto integration points with 24 fibers on the cross section.

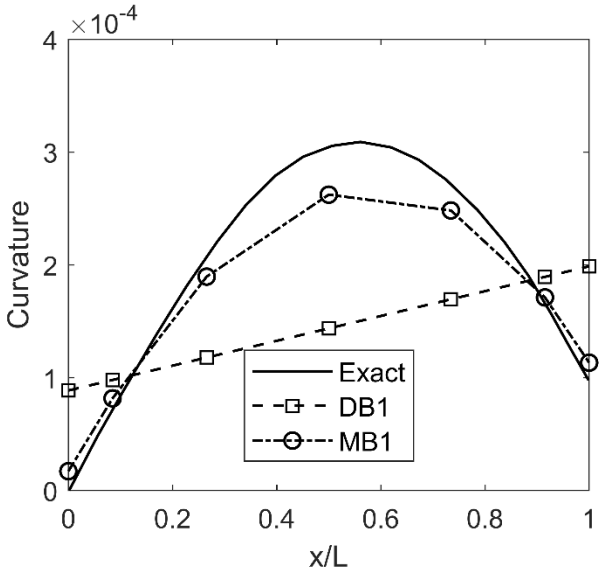

Figure 4. Curvature field along the member (1 element)

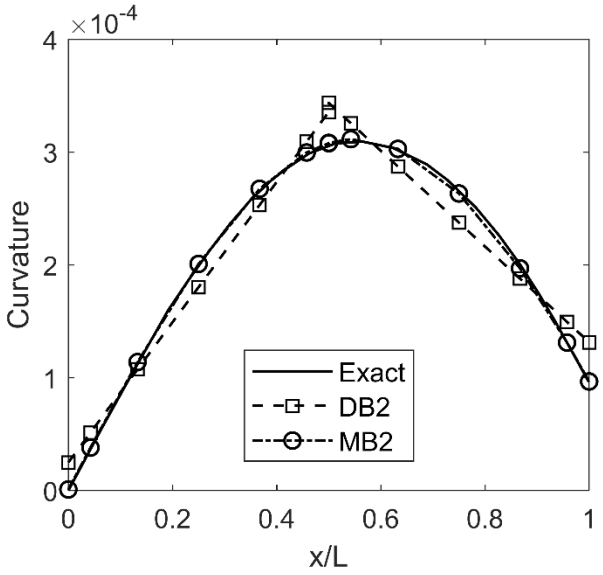

Figure 5. Curvature field along the member (2 elements)

2.5.2 Flexural-Torsional Buckling of Concentrically Loaded Angle Struts

This example, studied by Kitipornchai and Lee (1986), is about elastic flexural-torsional buckling of a pin-ended unequal-leg angle strut (L76x51x5 mm) under concentric loading. The detailed

material properties are: Young's modulus E = 200,000 MPa, Poisson's ratio v = 0.3, and yielding stress F_y = 312 MPa. The calculated elastic buckling load for members with different modified slenderness are shown Fig. 6. Here, the modified slenderness is defined as $\lambda = \sqrt{F_y/(\pi^2 E)}L/r_{min}$, where r_{min} is the minimum radius of gyration and L is the length of the angle strut. In Fig. 6, P_y is the section yielding load (squash load) and P_c is the applied axial load. It is seen that the buckling loads computed using the newly developed elements match well with the theoretical results given in Kitipornchai and Lee (1986).

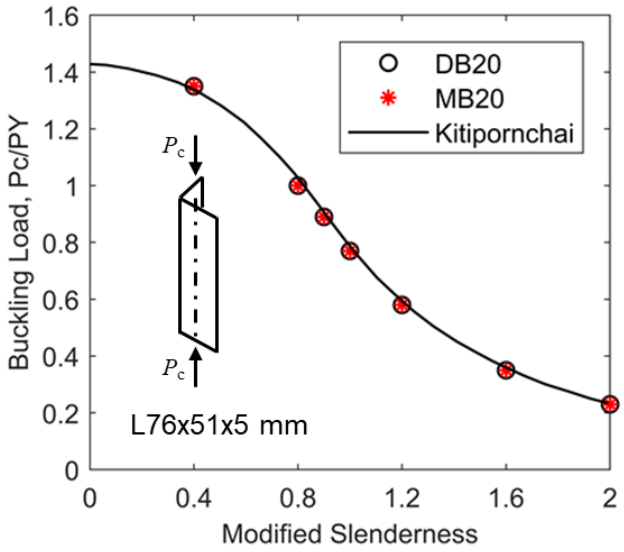

Figure 6. Flexural-torsional buckling of concentrically loaded angle struts (elastic)

As for inelastic buckling, Kitipornchai and Lee (1986) proposed an approximate residual stress distribution as shown in Fig. 7, which is also employed in the present study. An elastic-perfectly plastic stress-strain curve is used and the shear modulus is assumed to remain constant in the plastic region. The inelastic buckling loads of the angle struts with different slenderness are calculated using the new mixed and displacement-based elements, which are then compared with the values from Kitipornchai and Lee (1986) in Fig. 8. It is seen that the inelastic buckling loads also have very good agreement.

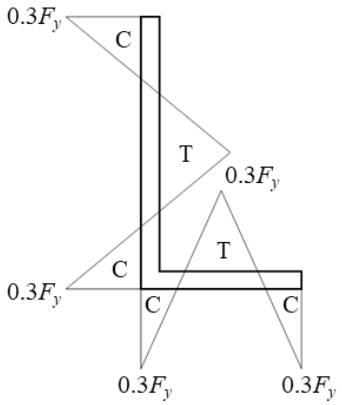

Figure 7. Assumed residual stress distribution for angle sections

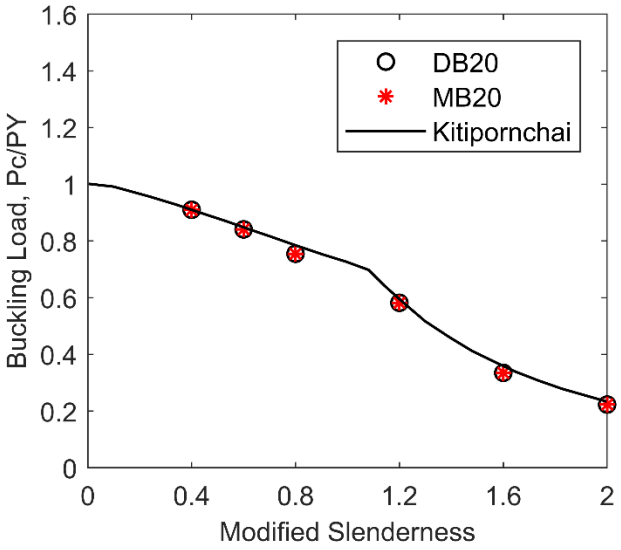

Figure 8. Flexural-torsional buckling of concentrically loaded angle struts (inelastic)

2.5.3 Nonlinear Dynamic Analysis of a Cantilever with Tee Section

Le et al. (2014) numerically studied the nonlinear dynamic response of a tee cantilever as shown in Fig. 9. The material properties are given as: $E = 210{,}000$ MPa, $\nu = 0.3$, and $\rho = 7850$ kg/m^3. The left end of the cantilever is totally fixed. Two concentrated loads ($P_y = -50P(t)$, $P_z = 25P(t)$) with different directions are applied to point O at the free end. The time history of $P(t)$ is given in Fig. 10. This example is analyzed using a time step of 0.001 s. Damping is not considered. The Z-displacement time histories of the free end centroid computed using the mixed and displacement-based elements are shown in Fig. 11, compared with the results given in Le et al. (2014), including the results of 40 corotational beam elements, 80 Abaqus B31OS elements and 2880 Abaqus isoparametric 20-node solid elements. The displacements computed using different elements agree well. The small discrepancies should be due to the fact that a consistent mass matrix is adopted in Le et al. (2014) while a lumped mass matrix is used in the present study.

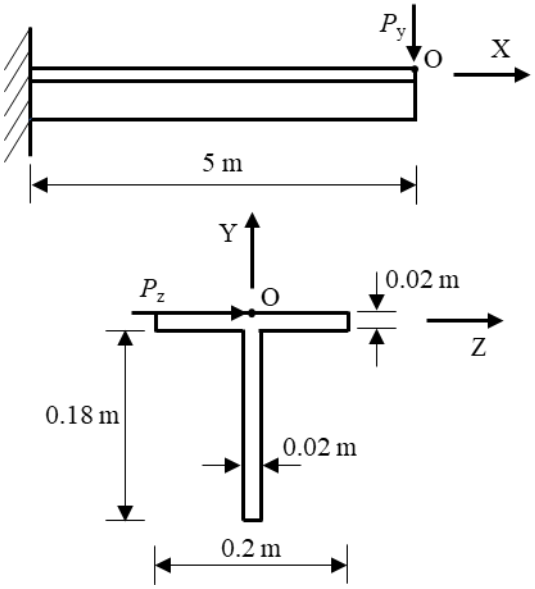

Figure 9. Cantilever with a tee section

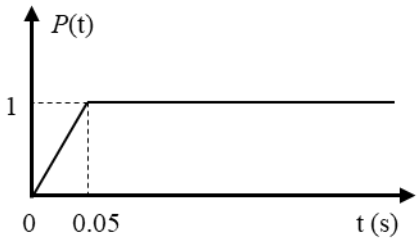

Figure 10. Time history of P(t)

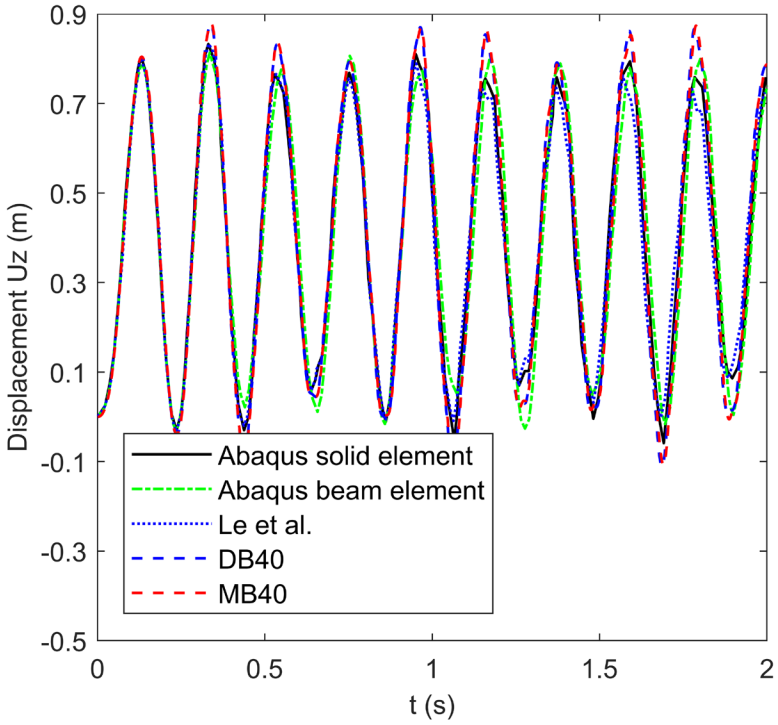

Figure 11. Time histories of the Z-displacement (Uz) of the right end centroid

3. Collapse Fragility Development of Transmission Towers Subjected to Hurricanes

3.1. Transmission Tower Modeling

An 18-meter transmission tower as shown in Fig. 12 is studied in this research. In the modeling of the tower, beam orientation assignment is of great importance due to the asymmetric angle sections. Therefore, Abaqus/CAE (Dassault Systèmes, 2017) is adopted as a finite element processor, as shown in Fig. 13(a). After each member being discretized into 3 elements, the Abaqus model is saved as an Abaqus INP file, which is then converted to an OpenSees input file. In addition, in Abaqus the beam orientation in the global system is defined using the directions of n1 and n2 (Fig. 13(b)); however, in OpenSees it must be defined using the direction of the principal axes (y and z in Fig. 13(b)). Therefore, a rotation matrix is adopted to obtain vectors y and z using the information of vectors n1 and n2. Primary members of the tower are made of ASTM A572 Grade 50 steel, while secondary members are made of ASTM A36 steel. The Steel01 material, a uniaxial bilinear constitutive model for steel, is used in OpenSees, where standard yield stresses are assumed and a strain-hardening ratio of 0.031 is adopted. Residual stress is considered by applying initial stress to each fiber on the cross section, which follows the assumed residual stress pattern as shown in Fig. 7.

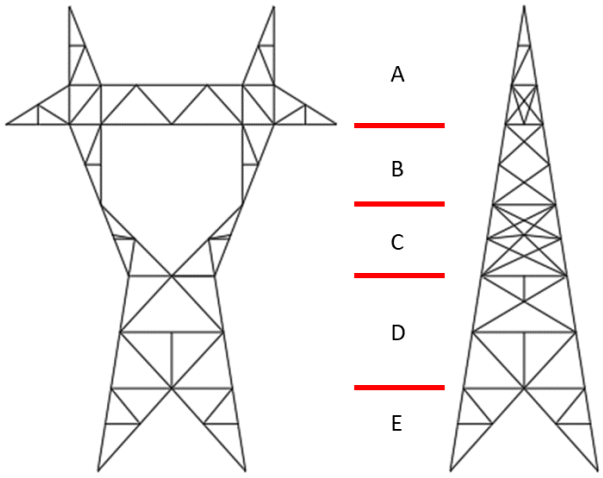

Figure 12. A typical transmission tower and its subsections

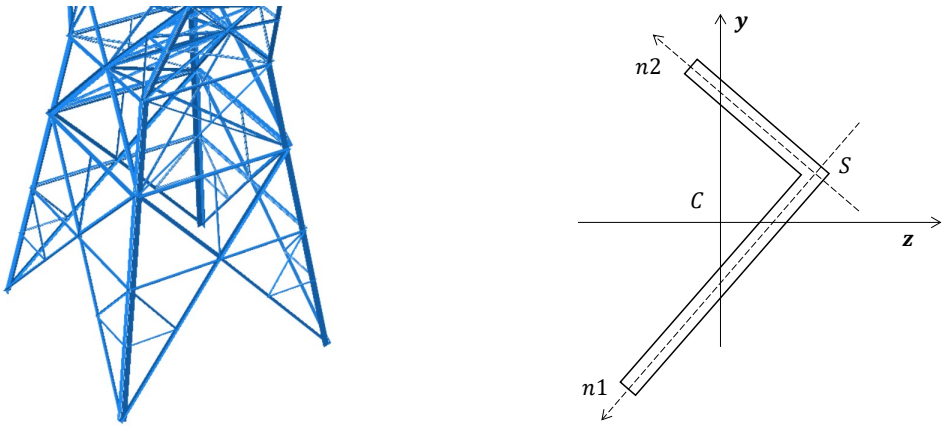

(a) (b)

Figure 13. (a) Transmission tower model in Abaqus (rendering beam profiles); (b) Section reference axes in Abaqus and section principal axes of an angle section

3.2. Hurricane Wind Records Selection

For the location of interest (latitude 41.776863, longitude -69.99792) studied in this research, 194 hurricane wind records are collected (see Du et al., 2022 for details) from a 10,000-year synthetic hurricane catalog given in Liu (2014). Nevertheless, conducting IDAs for all 194 records is computationally intensive so that it prohibits the collapse fragility analysis. Therefore, a good way is to reduce the number of records used while still cover the uncertainties in the wind records. As such, the collected 194 wind records are first divided into 4 clusters using the autoencoder neural network and k-means algorithm, and then a set of wind records are selected from each cluster (Du et al., 2022). After clustering, the number of hurricane wind records in each cluster are 27, 48, 56 and 61, respectively. The number of records selected from a cluster should be proportional to the total number of records in that cluster, which leads to 3, 5, 6 and 6 records from each cluster, respectively (see Fig. 14). This approach is adopted to ensure that the proportions of different patterns of wind records are similar in the original 194 hurricanes and the selected 20 ones. In Fig. 14 the wind speeds are resolved into the North and East directions because both the wind speeds and wind directions are time-variant. The selected 20 hurricane wind records are then adopted to calculate wind forces for collapse modeling using IDA.

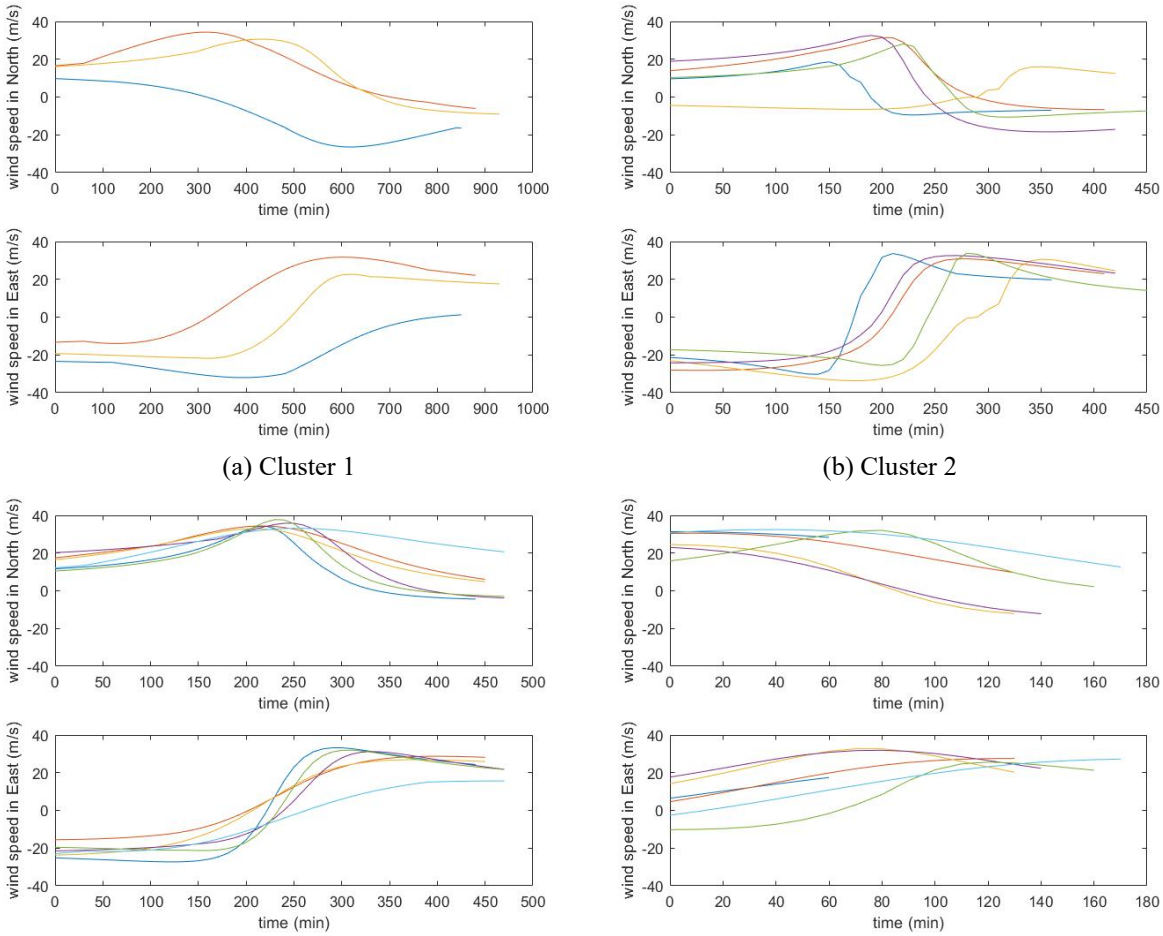

(a) Cluster 1 (b) Cluster 2

(c) Cluster 3 (d) Cluster 4

Figure 14. Selected hurricanes records

The selected wind records in Fig. 14 are 10-minute mean wind speeds at 10-meter height. Based on these wind records, the synthetic wind fields are developed, which consist of mean wind speeds changing along the height of the tower and the superimposed fluctuating winds. To avoid impulse effects in structural analysis, the first hour and last hour are added as the ramp-up and ramp-down as shown in Fig. 15(a). To run IDA, the 10-minute mean wind speeds are scaled gradually so that the storm-maximum 10-minute mean wind speed increases from 10 m/s to 55 m/s with a 5 m/s increment. The scaled mean wind speeds are then specified as the mean wind speeds at 10-meter height. To generate mean wind speeds at loading points of different heights along the tower, the logarithmic law for the atmospheric boundary layer is used. This means that the mean wind speed at 10-meter height is controlled, while the mean wind speeds at other heights are calculated using the logarithmic law. Open terrain with a roughness length of 0.03 m is assumed. Fluctuating wind is simulated using the Kaimal spectrum for representing the stochastic properties (Kaimal et al., 1972). As an example, Fig. 15(a) shows a set of generated wind speeds time histories without resolving to the North and East directions. The spectrum of the simulated fluctuating winds is presented in Fig. 15(b) together with the Kaimal spectrum.

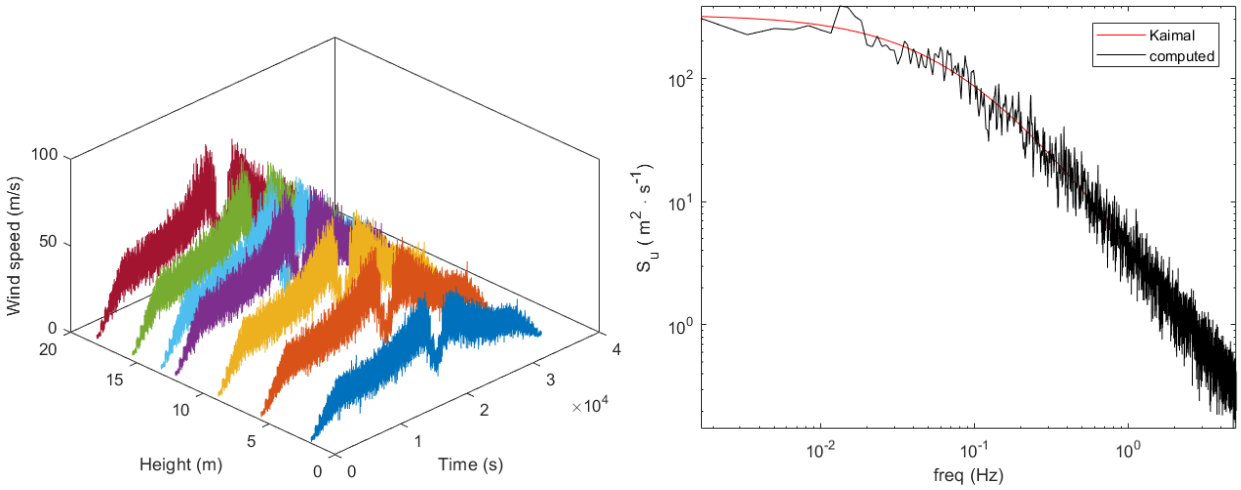

(a) (b)

Figure 15. (a) Simulated wind field; (b) Spectrum of fluctuating wind

3.3. Incremental Dynamic Analysis

The wind speed time histories on all loading points along the tower should be converted to dynamic wind loads for running IDAs. It is shown in ASCE 74 (Agnew, 2020) that the drag wind load on a tower section depends on factors like wind speeds, drag coefficient and projected area in the wind direction. Given that the drag coefficient varies as the tower configuration changes in the vertical direction, the tower is divided into 5 subsections along the height as shown in Fig. 12. The drag coefficient for each subsection can be calculated using the code equations. Considering the time-variant wind directions, the equations for yawed wind on transmission towers provided by ASCE 74 are adopted to calculated wind forces in both longitudinal and transverse directions as illustrated in Fig. 16. Note that Fig. 16 shows the wind force time histories on all five subsections, while the additional two times histories in the transverse direction are wind forces on ground wires and conductors.

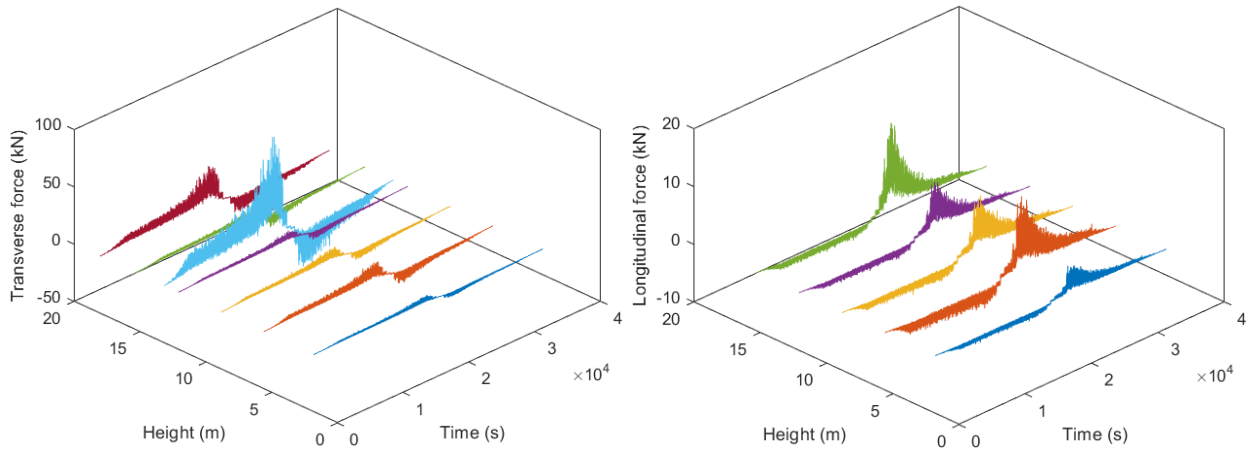

(a) Transverse force (b) Longitudinal force

Figure 16. Hurricane wind forces on the transmission tower

With the calculated wind forces from a suite of scaled wind records and the finite element model of a transmission tower in OpenSees, IDAs are conducted to estimate the collapse capacity of the tower. Here, collapse capacity is defined as the storm-maximum gust speed associated with the onset of collapse. The onset of collapse is defined as the slope of the IDA curve reaches 20% of

the elastic slope, which is borrowed from what is commonly used in earthquake engineering (Vamvatsikos and Cornell, 2002). The obtained IDA curves are shown in Fig. 17 along with the specified collapse capacities (red stars).

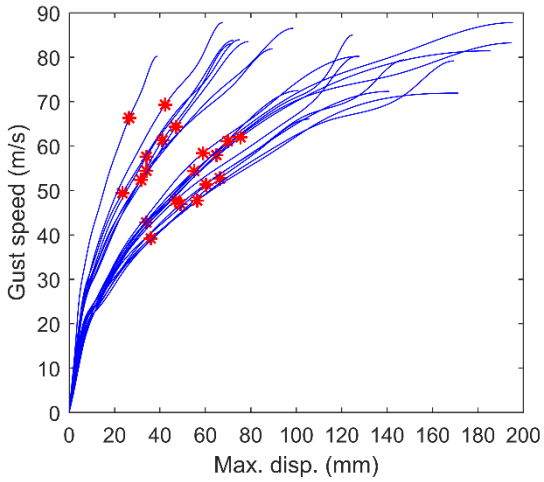

Figure 17. IDA curves with corresponding collapse points (red stars)

3.4. Collapse Fragility Development

Fragility is defined as the conditional probability of reaching a damage state for a structure subjected to a given intensity measure of the loading. In this research, collapse fragility of transmission towers is of interest. The collapse fragility in this work is defined as (Shinozuka et al., 2000)

$$F(IM) = \Phi\left(\frac{\ln\left(IM/\theta\right)}{\beta}\right) \tag{15}$$

where IM is the selected intensity measure for the fragility, i.e., the storm-maximum gust wind speed of a hurricane; Φ denotes the standard normal cumulative distribution function; θ is the median of the fragility function; β is the standard deviation of $\ln(IM)$. Eq. (15) implies that the collapse capacity IM_{collapse}, which represents IM values associated with the onset of collapse of a structure, follows a lognormal distribution (Baker, 2015). Parameters of fragility functions are estimated using the method of moments (Baker, 2015):

$$\ln(\hat{\theta}) = \frac{1}{m}\sum_{i=1}^{m}\ln(IM_{\text{collapse},i}) \tag{16}$$

$$\hat{\beta} = \sqrt{\frac{1}{m-1}\sum_{i=1}^{m}\left(\ln\left(IM_{\text{collapse},i}/\hat{\theta}\right)\right)^2} \tag{17}$$

where $\hat{\theta}$ and $\hat{\beta}$ are the estimates of parameters θ and β, respectively; m is the number of simulations (e.g., IDAs) considered; $IM_{\text{collapse},i}$ is the collapse capacity for the i^{th} simulation.

With the collapse capacity data from IDA curves (see Fig. 17), the two parameters (θ and β) defining the collapse fragility curve are estimated using Eqs. (16) and (17). The collapse fragility curve generated from Eq. (15) is shown in Fig. 18 together with the simulation data (black stars), which can be employed to quickly estimate the failure probabilities of transmission towers provided the storm-maximum gust speed is given. Only the uncertainties in the hurricane wind loads are considered in this research.

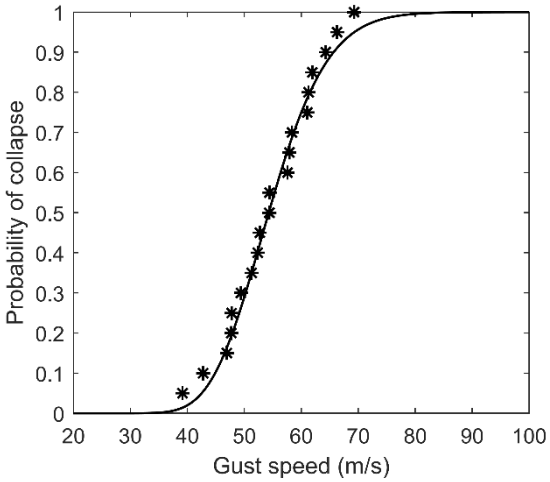

Figure 18. Fragility curve for the transmission tower along with the simulation data (black stars)

4. Conclusions

To model the collapse behavior of electrical transmission towers under dynamic loading, three-dimensional beam elements are developed within the OpenSees framework with capturing the geometric and material nonlinearities of angle members. The axial-flexural-torsional interaction behavior of angle members is simulated using the corotational total Lagrangian approach. The elements are validated with several examples. A procedure for developing collapse fragility curves under hurricanes is then proposed and demonstrated with an example. The fragility curve is expressed as the CDF of a random variable named collapse capacity, which is the storm-maximum gust wind speed at the onset of collapse. The uncertainties in collapse capacity are captured by running IDAs with a suite of selected hurricane wind speed and direction records. This means only the record-to-record randomness is propagated to the collapse capacity and thus to the fragility curve. Both changes in wind speed and wind direction are considered in this process.

Acknowledgments

The authors wish to thank Dr. Weichiang Pang for providing the synthetic hurricane catalog, and the DesignSafe project and the National Science Foundation for providing high-performance computing allocations. The authors also wish to thank Dr. Hao Sun and Mr. Robert Bailey Bond for their assistance in selection of the hurricane wind records. The material is based upon work supported by National Science Foundation under Grant No. CRISP-1638234 and Northeastern University. This support is gratefully acknowledged. Any opinions, findings, and conclusions expressed in this material are those of the authors and do not necessarily reflect the views of the National Science Foundation or other sponsors.

References

Agnew, F. (2020). “Guidelines for electrical transmission line structural loading.” *ASCE MANUALS AND REPORTS ON ENGINEERING PRACTICE NO. 74*, Reston, Virginia: American Society of Civil Engineers.

Alemdar, B. N. (2001). “Distributed plasticity analysis of steel building structural systems.” PhD Thesis, Georgia Institute of Technology, Atlanta, GA.

Baker, J. W. (2015). “Efficient analytical fragility function fitting using dynamic structural analysis.” *Earthquake Spectra*, 31(1), 579-599.

Cauffman, S. A., Phan, L. T., Sadek, F., Fritz, W. P., Duthinh, D., & Rossiter Jr, W. J. (2006). “Performance of physical structures in Hurricane Katrina and Hurricane Rita: A reconnaissance report.” *NIST Technical note 1476*, National Institute of Standards and Technology, Gaithersburg, MD.

Crisfield, M. A. (1991). “Non-linear finite element analysis of solids and structures (Vol. 1).” Chichester: John Wiley & Sons.
Crisfield, M. A. (1997). “Non-linear finite element analysis of solids and structures - Advanced Topics (Vol. 2).” Chichester: John Wiley & Sons.
Dassault Systèmes. (2017). “Abaqus standard and Abaqus documentation for version 2017.” Providence, RI: Dassault Systèmes Simulia.
Du, X., Hajjar, J. F., Bond, R. B., & Sun, H. (2022). “Collapse fragility development of electrical transmission towers subjected to hurricanes.” *Paper presented at the IABSE Symposium Prague 2022, Challenges for Existing and Oncoming Structures*, Prague, Czech Republic.
Kaimal, J. C., Wyngaard, J., Izumi, Y., & Coté, O. (1972). “Spectral characteristics of surface‐layer turbulence.” *Quarterly Journal of the Royal Meteorological Society*, 98(417), 563-589.
Kitipornchai, S., & Lee, H. (1986). “Inelastic buckling of single-angle, tee and double-angle struts.” *Journal of Constructional Steel Research*, 6(1), 3-20.
McKenna, F., Scott, M. H., & Fenves, G. L. (2010). “Nonlinear finite-element analysis software architecture using object composition.” *Journal of Computing in Civil Engineering*, 24(1), 95-107.
Vamvatsikos, D., & Cornell, C. A. (2002). “Incremental dynamic analysis.” *Earthquake Engineering & Structural Dynamics*, 31(3), 491-514.
Le, T.-N., Battini, J.-M., & Hjiaj, M. (2014). “Corotational formulation for nonlinear dynamics of beams with arbitrary thin-walled open cross-sections.” *Computers & structures*, 134, 112-127.
Liu, F. (2014). “Projections of future US design wind speeds and hurricane losses due to climate change.” Doctoral Dissertation, Clemson Univ., Clemson, SC.
Mattiasson, K., Bengtsson, A., & Samuelsson, A. (1985). “On the accuracy and efficiency of numerical algorithms for geometrically nonlinear structural analysis.” *Paper presented at the Europe-US Symposium on Finite Element Methods for Nonlinear Problems*, Trondheim, Norway.
Rasmussen, K. (1997). “Bifurcation of locally buckled members.” *Thin-Walled Structures*, 28(2), 117-154.
Rinchen, Hancock, G. J., & Rasmussen, K. J. (2020). “Geometric and material nonlinear analysis of thin-walled members with arbitrary open cross-section.” *Thin-Walled Structures*, 153, 106783.
Shinozuka, M., Feng, M. Q., Lee, J., & Naganuma, T. (2000). “Statistical analysis of fragility curves.” *Journal of engineering mechanics*, 126(12), 1224-1231.
Trahair, N. S. (1993). “Flexural-torsional buckling of structures (1 ed.).” Boca Raton: CRC Press.